3D Energy Harvester Evaluation

Vladimir JANICEK, Miroslav HUSAK

Dept. of Microelectronics, Czech Technical University in Prague, Technicka 2, 166 27 Prague, Czech Republic

janicev@fel.cvut.cz, husak@fel.cvut.cz

Abstract. *This paper discusses the characterization and evaluation of a MEMS based electrostatic generator, a part of the power supply unit of the self-powered microsystem [1], [3], [4]. The designed generator [2] is based on electrostatic converter [6] and uses the principle of conversion of non-electric energy into electrical energy by periodical modification of gap between electrodes of a capacitor [5]. The structure is designed and modeled as three-dimensional silicon based MEMS. With innovative approach we reached a very low resonant frequency of the structure (about 100 Hz.) The modified long cantilever spring design with minimum area of the chip, its ability to work in 3D mode, and the ability to be tuned to reach desired parameters, proves promising directions of possible further development.*

Keywords

MEMS, generator, characterization, energy, evaluation.

1. Introduction

The process of obtaining energy from the environment, converting it into consumable electricity, is generally known as energy harvesting. Devices using the principles of gathering energy are usually referred to as energy generators or energy harvesters [8], [9]. The main goal is to design the structure topology of the electrostatic generator in standard technologies available on the market. Structure based partly on basic beam structure is designed and modeled as three-dimensional silicon based MEMS. The main task is to optimize the dimensions of the structure due to the available production technology and to optimize the geometry of the structure itself with regard to the environment in which the generator will be used. Compared to already published proposals we expect to work in all 3 axes. This makes the system more effective to environment waste energy and makes it possible to use all energy available.

2. Electrostatic Harvesters

There are three topologies used as electrostatic energy harvesters. The main difference is in the sense of movement of the capacitor electrodes. The first one called

"In-Plane Overlap" (Fig. 1) creates capacitive differential vibrations in the plane of the device in the direction shown in Fig. 1. Maximum deflection is limited by finger length. The second type, known as "In-Plane Gap Closing" (Fig. 2) uses the same topology as the previous type, but the direction of the electrode is perpendicular to the direction of the type used in "In-Plane Overlap". The capacity change is directly proportional to the width of the gap between the electrodes. The last type "Out-of-Plane" (Fig. 3) is also based on the topology of the previous two solutions, but the direction of motion is perpendicular to the generator's surface. The oscillating movement of the electrode surface provides a change in capacity of a capacitor.
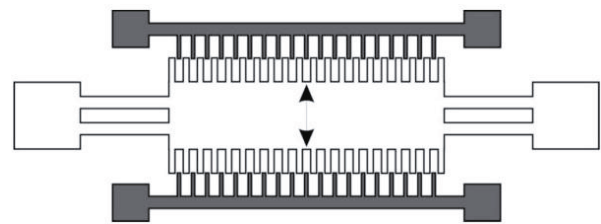
Fig. 1. In-Plane Overlap topology [7].
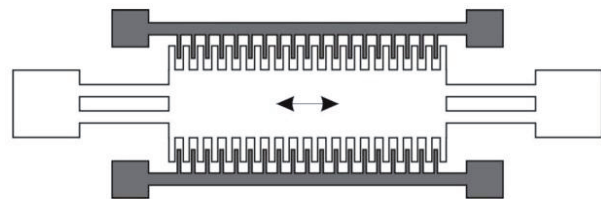
Fig. 2. In-Plane Gap Closing topology [7].

Fig. 3. Out-of-Plane topology [7].

3. Designing the Harvester

The designed power source uses a combination of electrostatic and piezoelectric generator (as required start-up power source) in the form of MEMS structures [5], [6]. Using CoventorWare we designed layout topology and 3D models. Using the harmonic analysis we obtained response to changes in the structure of the excitation signal.

Electrostatic generator uses the forces generated between the opposite charges on the plates of a charged capacitor. The basic generation-regeneration cycle is described in Fig. 4. Separation of charge Q on the electrodes depends on the potential difference. Voltage between them according to equation $Q = V.C_{VAR}$. C_{VAR} capacity is a function of geometry (topology) and electrode's properties of materials that surround them. Moving electrodes cause the capacity change between C_{MAX} and C_{MIN}. The amount of the extracted energy depends on how the variable capacity is connected to other electronic circuits. Two basic techniques are used to implement the electrostatic generator – switching or continuous mode.
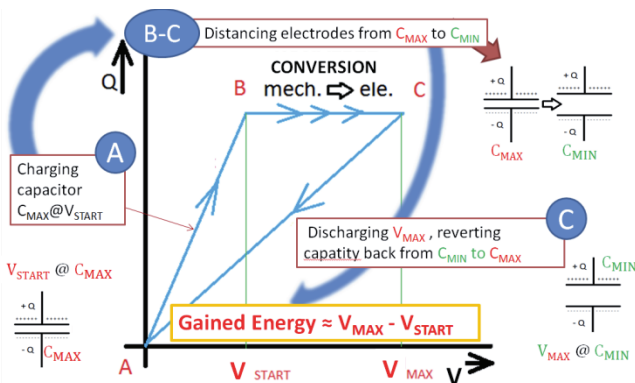
Fig. 4. Basic energy cycle of the electrostatic energy harvester.

4. Topology Design and Models

The CoventorWare was used to create layout topology, the 3D model, simulation net and to provide the electromechanical simulations.

The whole topology consists of 3 main parts (Fig. 5):

- Movable comb electrode,
- fixed electrodes,
- suspension beams.

The first two parts are paid attention only from the perspective of common areas in order to maximize surface capacitance density. The spring suspensions properties are crucial for many parameters of the resulting generator. The overall objective in the design topology of spring suspensions is their rigidity, minimum area, the distance between modal frequencies and amplitude (proportional to the magnitude of change).
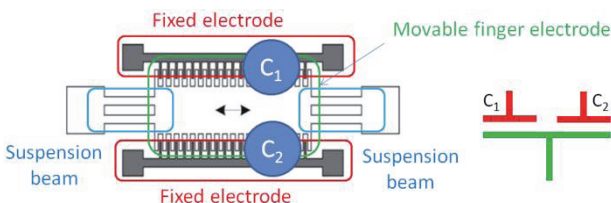
Fig. 5. Electrostatic energy harvester topology and model.

4.1 Suspension Beam Optimization

To achieve the minimum values of resonant frequencies of a spring suspension it is necessary to optimize its length, width and thickness. The length can be adapted to the available area on the chip, but other sizes have to be chosen in accordance with the manufacturing process and design kit.

Fig. 6 shows examples of optimized shapes of suspension beams. Tab. 1 shows the calculated values of resonant frequencies and length of the beam.
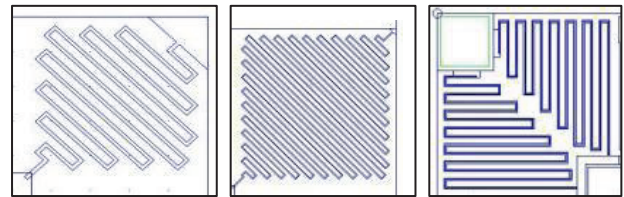
Fig. 6. Optimized suspension beams layouts (L1,L2,L3).

Our goal is to to achieve the lowest resonant frequency; therefore we need to build a very long cantilever formed spring suspension with the smallest possible footprint to keep the chip as small as possible.

Fig. 7 shows the optimized RTM Layout with very long beam based suspension springs.
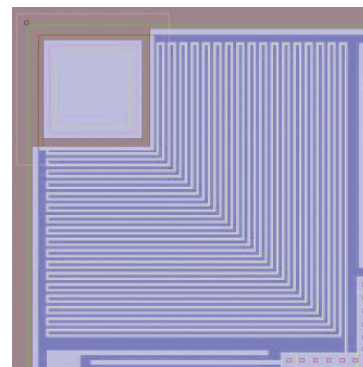
Fig. 7. Final suspension beams layout (L4).

The data in the table indicate the need for very long beam-shaped cantilever with minimum thickness and width. The last proposed version of the beam reaches the resonant frequency of 5.3 Hz (all data refer to simulations with the ideal enshrined beam).

	L1	L2	L3	L4
Number of arms (-)	14	38	14	33
Length (mm)	0,32	0,28	0,16	11
Resonant frequency (Hz)	11136	81	7647	5.3

Tab. 1. Suspension beams evaluation.

4.2 Mechanical Stress Optimization

Another important aspect is the mechanical stress (Fig. 8) inside the structure caused by mechanical vibrations. The most used method of hanging capacitor

structures in published papers is based on the topology of a simple bridge which is from one side firmly fixed to the frame chip and on the other side connected to the floating electrode. After exposure to mechanical vibration the movable electrode starts to swing. The maximum deflection depends on the frequency of oscillation, total weight and mechanical properties of the material and topology. The weight is generally to reduce the natural frequencies and increases the deflection and internal stress.

Simulation results (Fig. 9) indicate the maximum mechanical stress of 2.6 MPa under full scale of swing limited by stoppers. Since the maximum mechanical stress is lower than 0.5 times of yeild stress of silicon, the beam lifetime can be considered as almost infinite without fatigue phenomena.
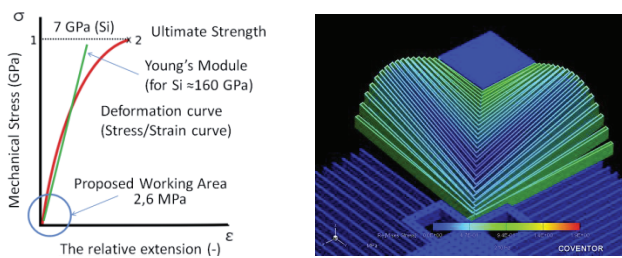
Fig. 8. Stress-Strain curve. **Fig. 9.** Stress simulation.

4.3 Final Layout

Fig. 10 shows the 9th version. The spring suspensions are formed as a periodic structure of the girder type. Thank to this we achieved such a suspension structure, which is mechanically equivalent to the suspension beam of great length, but on a much smaller effective area. Because of technological reason the position of two contact pads on solid electrodes had to be changed. Due to the asymmetrical position of spring suspensions to the moving electrode we obtained very little difference between the 1st and the 2nd modal frequency of the structure. In the case of fine oscillations there occurs a smooth transition from one type of conversion mechanism to another. This leads to increased efficiency and yield of the conversion cycle. The final 9th topology was sent to production foundry and was modeled for simulations.

5. Simulations

5.1 Modal Analysis

Modal analysis can be obtained from the natural resonance frequency of the mechanical system in equilibrium. On these frequencies the mechanically un-damped (lossless) system reacts to external motion excitation with unlimited deflection. The following figures show the mechanical simulations performed on the structure in CoventorWare. Fig. 11 shows the degree and
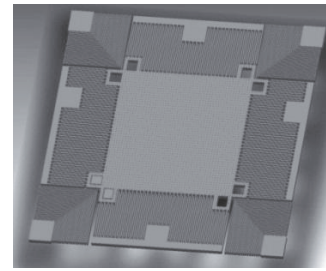
Fig. 10. 3D model of topology No.9 (only 2 stops visible).

direction of the deflection structure. For the function generator only the first 4 natural frequencies are important, because in them there is the greatest change in the position of movable electrode. Other natural frequencies are already showing the effect of several orders of magnitude smaller. The scale of deflection is multiplied due to small shifts and solid electrodes are not shown. Tab. 2 shows the first seven resonant (modal) frequencies.
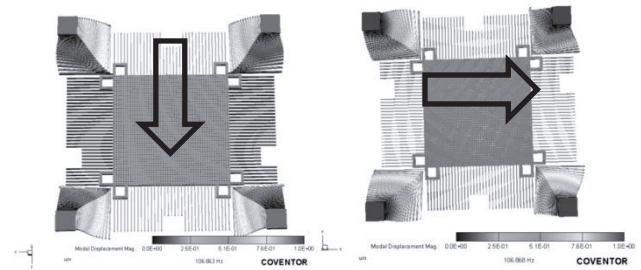
Fig. 11. 1st and 2nd modal frequency simulation.
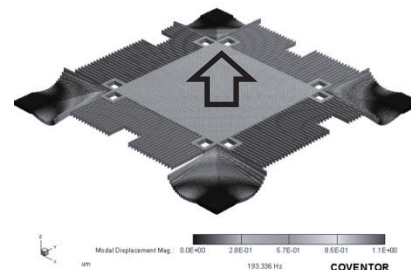
Fig. 12. 3rd modal frequency simulation.

Resonant frequencies	Frequency (Hz)
1	106.862678527832
2	106.867584228516
3	193.335723876953
4	214.255966186523
5	327.683410644531
6	328.238647460938
7	743.160461425781

Tab. 2. Simulated resonant frequencies.

From the table above we can see very low resonant frequencies of about 106 Hz and 193 Hz. The first three modes can be used for energy harvesting applications.

5.2 Harmonic Analysis

Using harmonic analysis, we want to find the dynamic response systems using harmonically variable load. Typically, a force on the structure in a particular direction (vector) is applied or the response of the structure to acceleration defined by magnitude and direction is monitored. Fig. 13 shows the mechanical response of the structure to nominal applied force in the direction of the X axis parallel to the surface of the generator. Frequencies are labeled as F1, F2, F3. In Fig. 13, displacements associated with the 1st and 2nd res. frequencies are larger than those at the 3rd res. frequency. This phenomenon is caused by the inertia mass which begins to act as a damping aspect at higher frequencies and the total deflection decreases. The maximum amplitude was reached at 1st res. frequency. This is caused due to the same direction of excitation amplitudes. For this reason, the chosen method of testing isn't appropriate for evaluation of the whole structure.
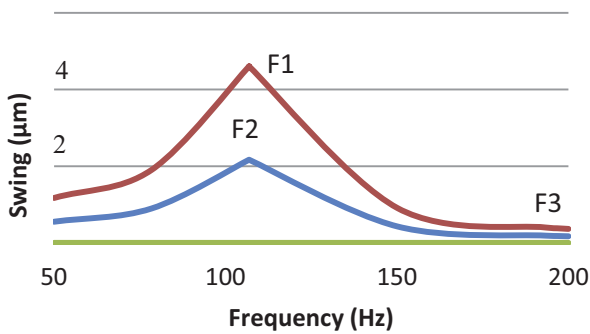
Fig. 13. Harmonic analysis – X axis excitation.

As mentioned above, we are looking for another method to test the mechanical behavior of structures independent of the direction of excitation initiative. Fig. 14 shows the mechanical response of the structure due to excitation accelerations in all three axes of 0.35 G. This testing doesn't affect the structure toward excitation, since this type of excitation can be considered directional. Fig. 14 shows a perceptible increase of the indicated level and the influence of the third resonant frequency. We can also see almost identical values of swing and displacement achieved on the 1st and 2nd resonant frequency.
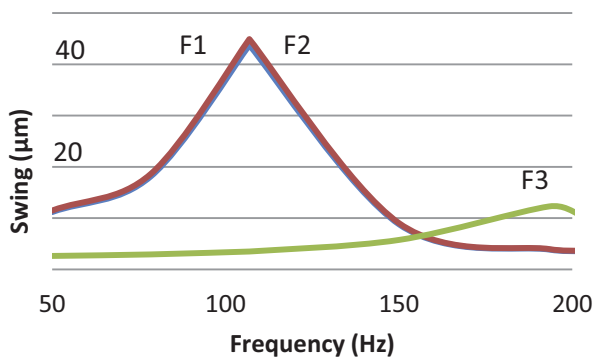
Fig. 14. Harmonic analysis – acceleration 0.35 G in all axes.

5.3 Capacitance Between Electrodes

The ideal design goal is to achieve very high ratio between the minimal and maximal capacitance. These values are limited by the maximal allowed movement of the floating electrode. This ratio of change is also directly linked to the energy output efficiency. The reached capacitance ratio is also influenced by movement directions and it changes with the different resonant frequency. Fig. 15 indicates the direction of applied force and the relative electrodes movement. Fig. 16 shows the dependence of the capacity value on electrodes movement in the direction which is parallel to the electrodes surface. The generator operates in the constant voltage mode so there are changes in the electrodes overlapping region with constant mutual distance. Simulations are carried out in the range of -10 to 10 µm. At the following pictures EL1-EL4 are fixed electrodes while CENTRAL indicates floating central electrode.
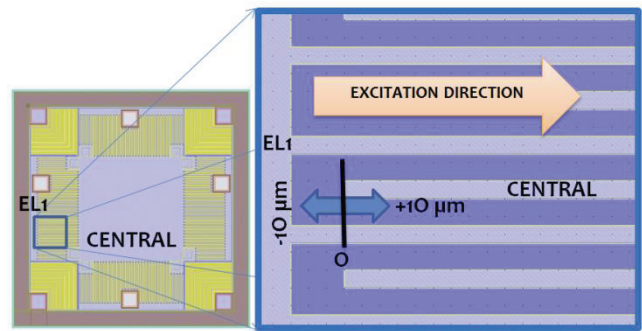
Fig. 15. Capacitance characterization (Linear).
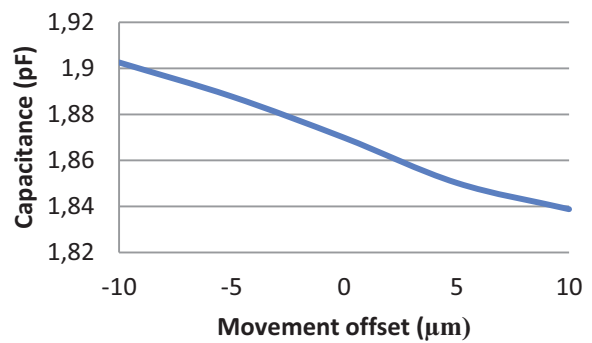
Fig. 16. Capacitance EL1/CENTRAL change.

On the graph in Fig. 16 it is clearly visible that the capacity decreases with increasing mutual shift of the electrodes. Fig. 17 shows the same structure, but this time we monitored the movement of the electrode EL2, which is perpendicular to the axis of movement. The excitation causes a relative movement of electrodes; this time under a constant charge when the surfaces of both electrodes move away from each other. The capacitance dependance is shown in Fig. 18.
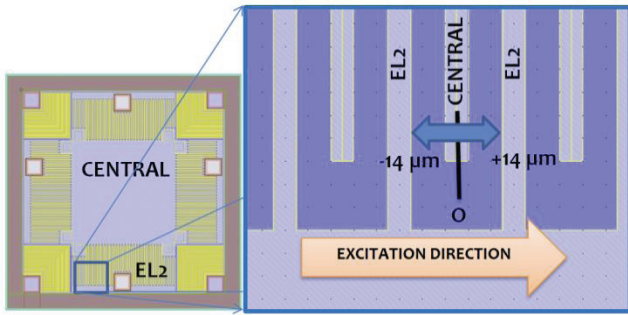
Fig. 17. Capacitance characterization (Perpendicular).
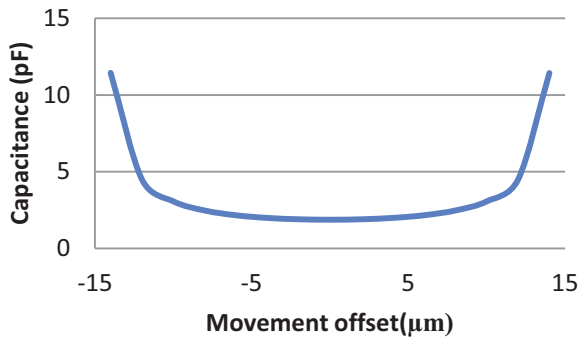
Fig. 18. Capacitance EL1/CENTRAL change.

The capacitor formed by a fixed electrode and a movable electrode EL2 shows in both limit states the maximum value of the capacity in comparison to the default value (resting position 0 in Fig. 17) where it is reduced to its minimum. The ratio of change of capacity is approximately 6.

Fig. 19a shows the relative position of the charge distribution and the dependence on the position of movable electrode EL1 and fixed electrode CENTRAL. Since the electrode EL1 moves exactly in the middle of the gap formed by the second electrode, the charge is distributed evenly on both sides. During the same movement the EL2/CENTRAL capacitor changes its gap dimension because of the perpendicular orientation of the device to the excitation movement direction. Fig. 19b shows one of the extreme cases of the relative positions of fixed electrodes and movable electrode EL2/CENTRAL. The electrodes operate under constant charge mode, as the distance between them changes, but overlap remains constant. In the figure the increase of the charge density is evident on one side of the electrode due to the shorter distance to the fixed electrode.
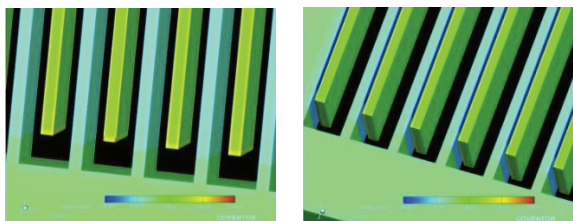
Fig. 19. Charge distribution on the EL1,2/CENTRAL based capacitor.

In terms of the mechanical stress acting on the structure is also important to know the actual conditions inside the structure when the device is not exposed to mechanical vibrations and the structure has only gravitational attraction. Assuming perfect anchorage of suspend beams ends, it is possible to perform a simulation of the behavior of the moving electrode, when there is only a gravity field influence without any other excitation forces. The weight of the fixed electrode causes a deflection in the spring hinges. The other simulation monitors the degree of this slack to be sure that there is no contact between the movable electrode and the chip substrate. Fig. 20 shows the shape of the moving electrode structure at rest position (in the Z axis scale is magnified by 30 for illustration).
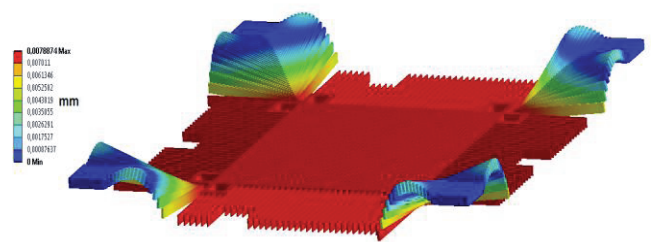
Fig. 20. Gravity force effect – deformation.

The scale of the graph shows the maximum sag of 7.8 µm, which could limit the movement of the electrodes. Because of the chosen manufacturing technology TRONICS which uses a 2 µm gap (BOX) between the lowest users defined structure and the chip substrate, the structure must be turned "upside-down" to let the movable electrode sag into space in a hermetically sealed 60 µm high cavity. The structure of the chip can be seen in Fig. 21. This makes it possible to use the proposed structure at both first two resonant frequencies without any mechanical limitations.
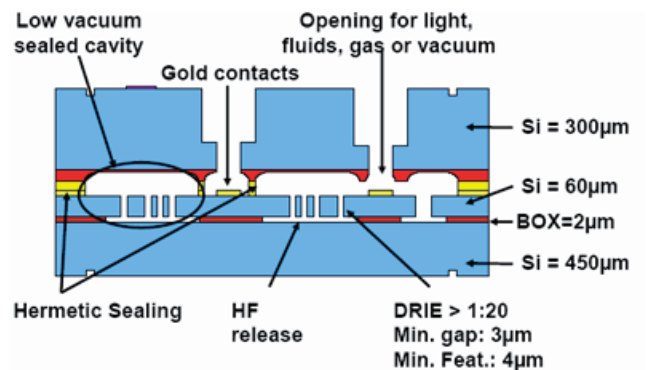
Fig. 21. Manufacturing technology TRONICS.

Optimal state can be achieved by adjusting a spring hinge stiffness. This would lead to the symmetric amplitudes in the Z direction and suspension travel approximately 30 µm, i.e. to half the height of the electrodes. However, this slack would limit the capacity size and the resulting effectiveness of the structure at oscillations around the 1st and the 2nd natural frequency.

6. Fabrication

The proposed generator was produced by SOI HARM 60 μm Tronics® technology. Fig. 22 and 23 show details of the laboratory sample.
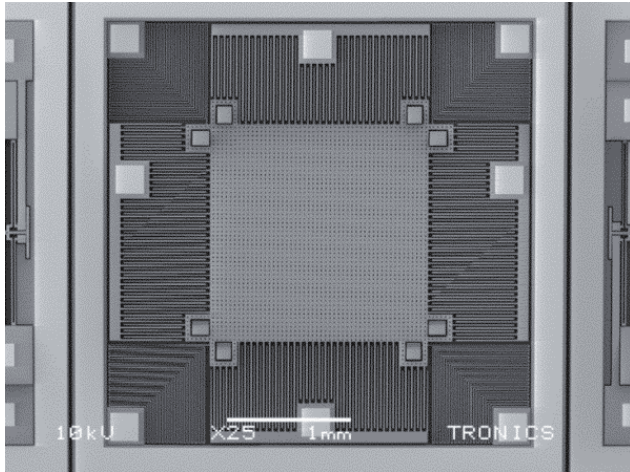
Fig. 22. Real sample of energy harvester.
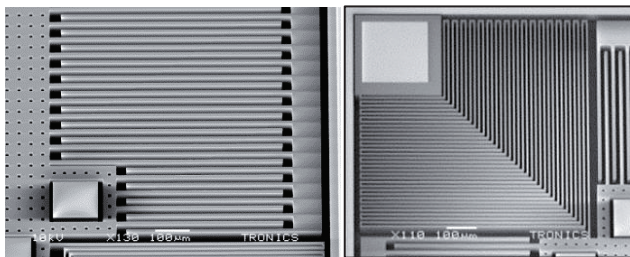
Fig. 23. Details of real sample of energy harvester.

7. Characterization

Wiring diagram of the measuring chain is shown in Fig. 24. Capacitive H-bridge consists of a single capacitor with variable capacity (capacitor structure in the generator) and three ceramic capacitors with a capacity of 10 pF. The structure is supplied with periodic sinusoidal signal from the function generator.
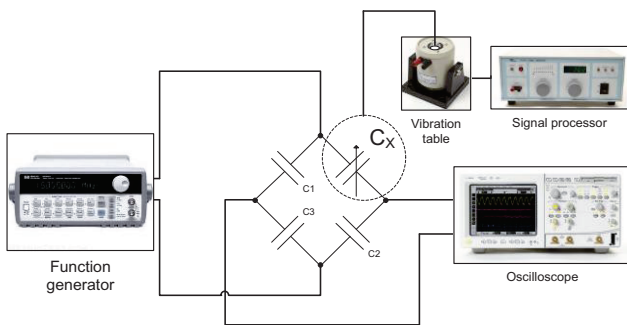
Fig. 24. Measurement chain for generator characterization.

Test board with H-bridge (Fig. 26a) is placed on a vibration table KCF ES02. The mechanical oscillations

(frequency and amplitude) are controlled by a signal generator and a power amplifier PA5100 KCF (Fig. 25). The signal output from the bridge is displayed on the oscilloscope. To measure the acceleration I we used an calibrated accelerometer (Fig. 26b).
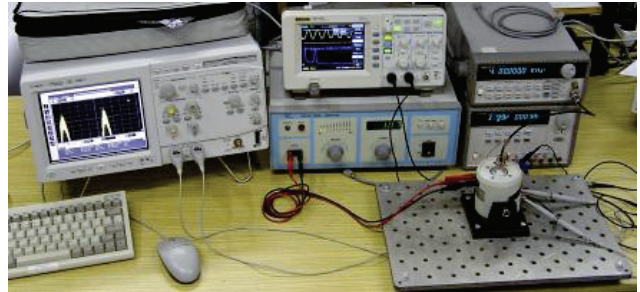
Fig. 25. Lab Equipment for generator characterization.
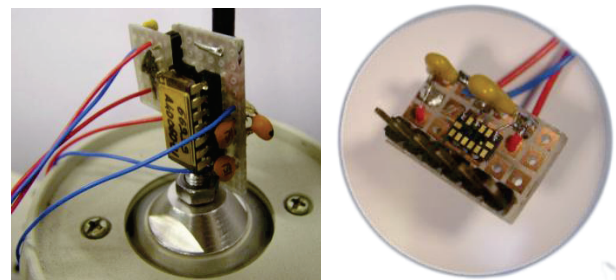
Fig. 26. (a) Testing PCB, (b) Accelerometer PCB.

7.1 Resonant Frequency Evaluation

Changing the capacitance of the variable capacitor placed on the chip leads to a periodic change of the amplitude of the output signal. This phenomenon can be seen in the form of a modulation envelope on the output signal. The base frequency of the signal is equal to the input frequency on the bridge (4 kHz). In Fig. 27 the modulated signal f_{INP} with the envelope which is equal to the modulating signal f_{MOD} can be seen. A ripple frequency of approx. 100 Hz is apparent, which corresponds to the first resonant frequency of the structure.
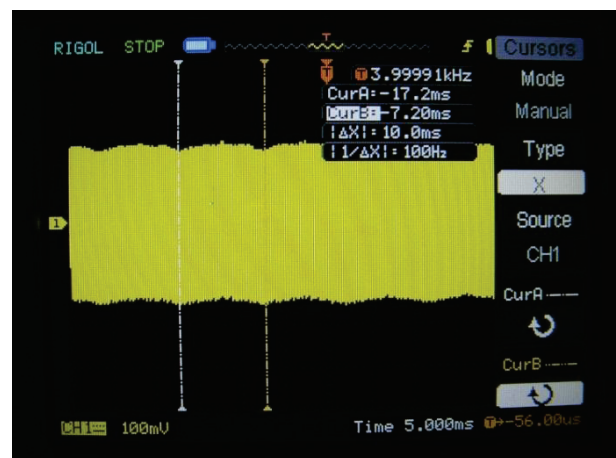
Fig. 27. Bridge output signal with visible envelope (100 Hz).

An excitation frequency of 4 kHz has been used because up to approx. 1.6 kHz bridge showed strong frequency dependence on excitation frequency. Higher frequency could be limited by the electrical parameters of wires used for the measurement. Measured data has been analyzed in the frequency domain (FFT analysis).

After reaching 100 Hz a visible spectral line corresponding to the 1st resonant frequency appeared. This phenomenon is shown in Fig. 28. In the right part of the figure the excitation signal of 4 kHz can be seen. The scale on the time axis had to be increased for better reading of values, so the excitation signal frequency appears to be "wide".

Fig. 28. Spectral analysis; 1st res. frequency peak visible.

The generator was positioned so that the movement occurred for mutual approaching and distancing of the plates, corresponding to the constant charge mode when the generator reaches maximum ratio between the values of C_{MAX} and C_{MIN}. After increasing the frequency of the mechanical excitation, the spectral line dissapeared again and the amplitude went down.

7.2 Capacitance Evaluation

A LCR bridge was used for evaluation of C_{MIN} value. Dependence of the C_X on the angle of rotation can be seen in Fig. 29.
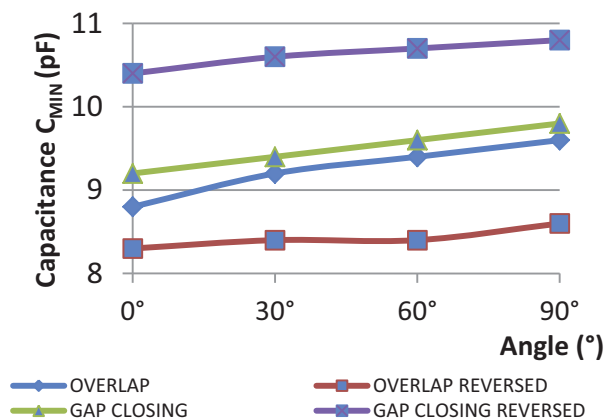
Fig. 29. C_{MIN} dependence on the angle.

The "reversed" topologies are working "upside down" as described before, i.e. chip is rotated by 180° in the vertical direction. This effect causes a small decrease in the whole curve compared to others.

7.3 Linearity Evaluation

A linearity of the response to the amplitude of the generator excitation was evaluated. With gradually increasing amplitude (generator KCF PA5100) of the vibration excitation the brifge output voltage was observed. We expect a linear progression until reaching such mechanical displacement that will be limited by in-build stops inside of the structure. Fig. 30 describes the dependence of the overshoot amplitude (the difference between maximum and minimum amplitude of the envelope of excitation signal).
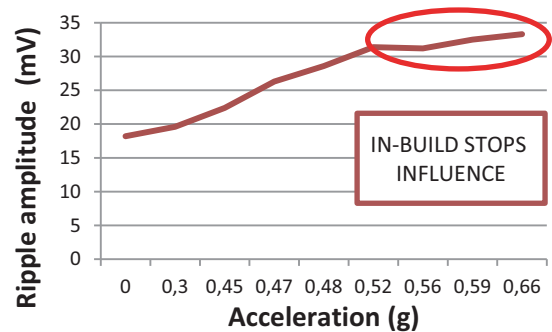
Fig. 30. Deflection lineariry.

In Fig. 30 a point is visible where increasing acceleration no longer leads to an increase in the amplitude of the output signal envelope. This demonstrates the efficacy of mechanical stops built in the structure of the generator. This phenomenon occurs at. 0.5 g.

7.4 Output Power Evaluation

The next step was to test the function of the energy generator. However, because the discrete form of measurement and limitations of discrete components in form of parasitic capacity or leakage currents, we verified the functionality through finding maximum achievable ripple. This is equivalent to changing the values of C_{MIN} and C_{MAX}. The generator was mechanically actuated at 103 Hz, which corresponds to the first resonant frequency and acceleration of 0,7 g. A deflection, which corresponded to a maximum change of capacity, was observed.

Maximum achievable amplitude ripple reached a size of 35.2 mV (Dot A in Fig. 31). Knowing the values of C_{MIN} and C_{MAX} (value taken from simulations) the capacity change was determined. According to the deducted amplitude a charge change was determined (1). Furthermore, it is possible to directly calculate the output power and change in performance due to the charge per unit time (calculated from the excitation frequency) (2).

$$\Delta Q = \Delta C \cdot \Delta U = 6.5 \cdot 10^{-12} \cdot 35 \cdot 10^{-3} = 227 \cdot 10^{-15} \, \text{C}, \quad (1)$$

$$P = \frac{W}{T} = f \cdot \Delta Q = 103 \cdot 227 \cdot 10^{-15} = 23.4 \, \text{pW}. \quad (2)$$

The measured output power is 23.4 pW. But it is necessary to take into account that due to the very small changes in the measured values and capacities it is necessary to consider the influence of parasitic capacitance and resistance of the measuring equipment (oscilloscope probes). Fig. 31 shows the influence of parasitic effects devices (surge capacity and leakage current) on the amplitude of the output signal.
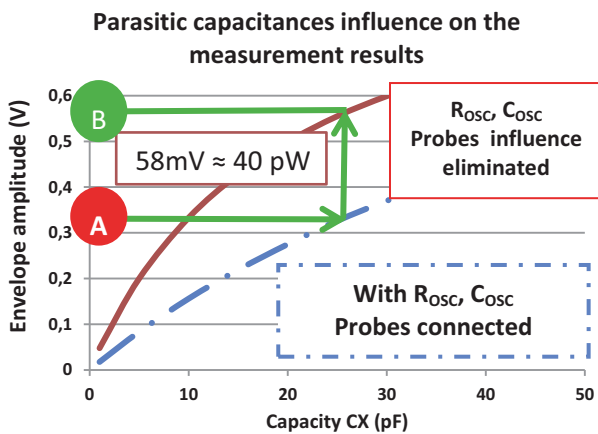
Fig. 31. Parasitic effects elimination.

The dot-and-dash code in Fig. 31 shows the decreased output amplitude caused by connected probe with 20 pF/1 MΩ (parameters of real osciloscope probe). After numerical correction of the influence of the probe the generators output voltage has reached 58 mV (Dot B in Fig. 31). This voltage corresponds to (according to (2)) the power of 40 pW.

8.　Comparison and Conclusions

Tab. 3 shows simulated and real parameters of the proposed generator.

Parameter	Simulations	Real Sample
1st resonant frequency	106 Hz	103 Hz
C_{MIN}	2 pF	8pF (package)
In-build stops effect	Starts at 0.35 g	ca. 0.5 g
Power density	10 μW.cm^{-3}	3 μW.cm^{-3}

Tab. 3. Simulated vs. real sample properties.

The measured parameters show a very good conformity with the simulated model. Output power reaches a value of 1/3 of the simulated one but it is necessary to keep in mind that the proposed generator will be integrated and in such form there will be much better results. The differences in parameters are mainly caused by parasitic effect of the chip package and leakage currents of the probes. We expect to integrate this in the future to get better results.

Acknowledgements

References

[1] JANICEK, V., HUSAK, M. Self-powered microsystems with PVDF based microgenerator. In *IMAPS 2007 Proceedings*. Washington (USA), 2007. p. 953 - 957.

[2] JANICEK, V., HUSAK, M., JAKOVENKO, J., FORMANEK, J. Design and fabrication of 3D electrostatic energy harvester. *Radioengineering*, 2012, vol. 21, no. 1, p. 231 - 238.

[3] FRY, D. N., HOLCOMB, D. E., MUNRO, J. K., OAKES, L. C., MASTON, M. J. *Compact Portable Electric Power Sources (report ORNL/TM-13360)*. Oak Ridge (USA): Oak Ridge National Laboratory, 1997.

[4] BEEBY, S. P., TUDOR, M. J., WHITE, N. M. Energy harvesting vibration sources for microsystems applications. *Journal of Measurement Science and Technology,* 2006, vol. 17, no. 12, p. 175 - 195.

[5] MARZENCKI, M., BASROUR, S., CHARLOT, B., GRASSO, A., COLIN, M., VALBIN, L. Design and fabrication of piezoelectric micro power generators for autonomous microsystems. In *Proceedings of Symposium on Design, Test, Integration and Packaging of MEMS/MOEMS DTIP05.* Montreux (Switzerland), 2005, p. 299 - 302.

[6] STERKEN, T., FIORINI, P., BAERT, K., BORGHS, G., PUERS, R. Novel design and fabrication of a MEMS electrostatic vibration scavenger. In *Power MEMS Conference*. Kyoto (Japan), 2004, p. 18 - 21.

[7] ROUNDY, S., WRIGHT, P., PISTER, K. Microelectrostatic vibration-to-electricity converters. In *Proceedings of ASME International Mechanical Engineering Congress & Exposition (IMECE)*. New Orleans (USA), 2002, p. 1 - 10.

[8] ROUNDY, S. *Energy Scavenging for Wireless Sensor Nodes with a Focus on Vibration to Electricity Conversion*. Ph.D. Dissertation. Berkeley (USA): University of California, 2003.

[9] SODANO, H., INMAN, D., PARK, G. A review of power harvesting from vibration using piezoelectric materials. *The Shock and Vibration Digest*, 2004, vol. 36. p. 197 - 205.

About Authors...

Vladimír JANÍČEK was born in Most in 1974. He received his M.Sc. from Dept.of Microelectronics FEE CTU in Prague in 2000. Ph.D. in 2012. Assistant Professor at the Department.

Miroslav HUSÁK was born in Kladno in 1953. He works as a Full Professor at the Dept. of Microelectronics FEE CTU in Prague since 2000, manages the Microsystems Group. His research is focused in the field of microsytems and integrated sensor systems.